出國報告（出國類別：參加國際研討會）

第 32 屆太空科技與科學國際研討會
The 32nd International Symposium on Space Technology and Science

服務機關：國防大學理工學院動力及系統工程系
姓名職稱：陳幼良　教授
派赴國家：日本
出國期間：**108/06/14~108/06/22**
報告日期：**108/06/26**

摘要

本次參加之國際研討會為第三十二屆太空科技與科學國際研討會(32nd International Symposium on Space Technology and Science (32nd ISTS)，於 6 月 15-21 日假日本福井縣福井市(AOSSA and Happiring)舉行，大會以“如鳳凰般飛翔至太空(Fly like a Phoenix to Space) 為主題。計有全體會議講座、技術會議、論文發表、學生會議、太空展覽以及參觀福井市傳統文化節目等事項。6 月 17 日 0900-1000 時由日本宇宙航空研究開發機構 Yasuhiro Morita 教授擔任主席，主持大會開幕式典禮。6 月 17 日 1000-1800 時由太空人 NASA Astronaut Sandra Magnus 等人員實施全體講座分享。當晚 1900 時參加 ISTS 開幕歡迎宴會。6 月 18 日開始依大會規劃之場地區分各研究技術議題，實施分組報告研討與意見交流。6 月 15 日 1200 時開始為期 5 天的國際太空展博覽會，陳展內容是日本宇宙航空研究開發等各部門機構，為負責日本航空太空開發政策的國家研究與發展法人，包括研究、開發和發射人造衛星、探測小行星和未來可能的登月工程，其他參展廠商業務範圍相當廣泛。超過 1,000 名參與會議的論文發表者及聽講者(包含學者教授、研究生、產業界研究人員）遍及世界各國，ISTS 研討會探討領域甚廣，是一個關於太空技術和科學的國際研討會，涵蓋了與空間有關的幾乎所有學科，舉凡太空領域的航空器、火箭和衛星等等均涵蓋在內。

本次會議投稿篇數為 1,000 餘篇，學術討論範圍計有：化學推進和吸氣式發動機、材料與結構、航天動力學，導航制導與控制、流體動力學和氣動熱力學、小衛星、航天運輸、微重力科學與技術、熱控、衛星通信廣播和導航、科學和技術促進人類與機器人太空探索、探空火箭、地球觀測、太空生命科學、航天動力系統、太空環境和碎片、系統工程和信息技術、航天教育和推廣為全民利益、太空法律，政策和國際合作、安全與任務等 20 幾項主軸，極為豐富。

此行獲邀發表“Impact Behavior of a Functionally Graded Ceramic Composite Based on Derived Theoretical Analysis Model”。本研究之 Al_2O_3/ZrO_2 三層功能梯度陶瓷複合材料係以粉末冶金法製作而成，各層厚度均為 3 mm，且由厚度為 1 mm 及 4 mm 的 6061-T6 鋁合金背板搭配製成。理論分析模型的啟發來自於 Tate 理論及 Zaera 理論，可用於評估和研究此樣品受衝擊時的行為，並使用彈道實驗來驗證此結果。本研究整合了彈頭的侵蝕、陶瓷材料的破碎以及金屬背板的變形，進而建立彈頭垂直衝擊的理論分析模型。針對陶瓷部份，考慮了破裂陶瓷錐的體積和抗壓強度的變化。關於金屬背板的變形，考慮了塑性變形功、外力功及其動能守恆原理，並依據背板的厚度，區分為沖塞型與花瓣型等兩種破壞模式，最後藉由 MATLAB 常微分方程式功能函式 ode 45 求解相關的常微分方程。依據 NIJ 標準 IV 級，本研究彈道實驗使用 0.30″穿甲彈(AP)執行彈道測試，顯示理論分析模型的預測結果與彈道實驗測試結果有一致性。

目次

目的

1.赴日本福井縣福井市參加第三十二屆太空科技與科學國際研討會，發表研究成果。
2.擔任議程主持並與國際學者進行學術交流。
3.觀摩日本宇宙航空工業的發展。

過程

此次研討會於 6 月 15~21 日假日本福井縣福井市(AOSSA and Happiring)舉行，計有全體會議講座、技術會議、論文發表、學生會議、太空展覽以及參觀福井市傳統文化節目等事項。6 月 15 日 1200 時開始為期 5 天的國際太空展博覽會， 6 月 17 日 0900-1000 時由日本宇宙航空研究開發機構 Yasuhiro Morita 教授擔任主席，主持大會開幕式典禮。6 月 17 日 1000-1800 時由太空人 NASA Astronaut Sandra Magnus 等人員實施全體講座分享。當晚 1900 時參加 ISTS 開幕歡迎宴會，並由福井縣縣長杉本達治主持開幕，參與開幕貴賓計福井市市長東村新一、ISTS 委員會會長、東京大學鈴木晃一郎教授、宇宙航空研究開發機構理事長、日本航空宇宙學會會長等。並準備精緻餐點、精彩書法演出和日本當地民俗三味線等表演，另介紹和提供當地名產蕎麥麵和清酒。6 月 18 日開始依大會規劃之場地區分各研究技術議題，實施分組報告研討與意見交流。為期 5 天的“International Space Exhibition”陳展博覽會，陳展內容是日本宇宙航空研究開發等各部門機構，為負責日本航空太空開發政策的國家研究與發展法人，包括研究、開發和發射人造衛星、探測小行星和未來可能的登月工程，其他參展廠商業務範圍相當廣泛，涵蓋交通運輸、船舶、航空太空、鐵路車輛、武器、軍事裝備、電動馬達、發動機、能源、空調設備等各種機械機器設備之生產製造。日本衛星拍攝到的月球表面照片，有 8K 的解析度，令人印象深刻。

6 月 18 日聽取由日本國防科學院航空航天工程系 Hiroaki Tanaka 發表“Numerical Simulation on Harpooning a Metal Anchor for Capturing Space Debris”，內容為研究金屬錨的穿透行為的數值模型，並證明其適用性，此項研究採用兩種類型的有限元網格-三角形棱柱和六面體-並進行數值模擬，將模擬結果與固定和自由下落目標的實驗結果進行了比較，結果顯示使用三棱柱網格

可以精確模擬穿透行為。此外，還研究了一些材料模型發現，Johnson-Cook 模型可用於模擬將金屬錨固定到碎片結構的穿透行為，標準誤差僅百分之幾。日本東京城市大學 Yuim Fujimori 發表“Study on Topology and Stability of Cable Network”，內容為在傳統的研究中，在電纜邊緣形成的凹陷是設計電纜網絡的重要因素之一，張力可以通過下垂的比例來控制。然而，與電纜伸長剛度相關的下垂率的設計尚未闡明，因此，此項研究還驗證了電纜剛度和垂度比之間的關係，描述了電纜網絡結構的設計方法。

6 月 19 日聽取九州工業大學綜合系統工程應用科學系 Farhan Abdullah 發表“n-Situ Monitoring of Carbon Fiber/Polyether Ether Ketone (CF/PEEK) Composite Thermal Expansion in Low Earth Orbit”。內容為在研究中討論了空間暴露實驗的設計，該實驗允許原位測量 LEO 中 CF / PEEK 複合材料樣品的熱膨脹係數（CTE）的變化，本研究中還將展示在發布之前進行的地面測試，該實驗通過將結果傳輸到地面消除了對樣本檢索的需要，該實驗是 Ten-Koh 衛星上的有效載荷，使用附有應變儀和溫度傳感器的 CF / PEEK 樣品來測量 CTE 的變化， CF / PEEK 樣品外部連接到衛星結構的頂部，初步結果顯示，空間暴露實驗可以測量計算 CTE 值所需的應變和溫度變化。日本宇宙航空研究開發機構 Akihisa Uematsu 發表“Performance Evaluation of Camera-based Displacement Measurement for Space-borne Structures”。內容是在這項研究中，基於 8 點算法和兩台攝像機拍攝的立體圖像，用地面實驗評估了位移測量的性能，在航天器或衛星上，諸如結構安裝位置和兩個攝像機之類的約束條件影響目標，第一攝像機和第二攝像機以及視野之間的相對距離，檢查兩台攝像機之間的距離與測試儀器位移的測量誤差之間的關係。

6 月 20 日獲邀發表“Impact Behavior of a Functionally Graded Ceramic Composite Based on Derived Theoretical Analysis Model”。本研究之 Al_2O_3/ZrO_2 三層功能梯度陶瓷複合材料係以粉末冶金法製作而成，各層厚度均為 3 mm，且由厚度為 1 mm 及 4 mm 的 6061-T6 鋁合金背板搭配製成。理論分析模型的啟發來自於 Tate 理論及 Zaera 理論，可用於評估和研究此樣品受衝擊時的行為，並使用彈道實驗來驗證此結果。本研究整合了彈頭的侵蝕、陶瓷材料的破碎以及金屬背板的變形，進而建立彈頭垂直衝擊的理論分析模型。針對陶瓷部份，考慮了破裂陶瓷錐的體積和抗壓強度的變化。關於金屬背板的變形，考慮了塑性變形功、外力功及其動能守恆原理，並依據背板的厚度，區分為沖塞型與花瓣型等兩種破壞模式，最後藉由 MATLAB 常微分方程式功能函式 ode 45 求解相關的常微分方程。依據 NIJ 標準 IV 級，本研究彈道實驗使用 0.30″穿

甲彈(AP)執行彈道測試，顯示理論分析模型的預測結果與彈道實驗測試結果有一致性。當日本人也應邀擔任一場次發表會(Session c-12 Structural Materials 1)的主持人。

福井縣擁有豐富而美麗的大自然，文化和傳統產業在福井悠久的歷史中得到了發展，並一直傳承至今。福井還為長壽，健康的生活提供了最佳環境。福井縣為太空探索事業提供了豐富的資源，該縣為重工業製造商提供了優越的地理位置，這些製造商提供用於許多太空任務的必要設備。衛星項目正在進行中，與各省的工業、大學和地方政府密切合作，目標於在 2020 年發射小型衛星。

福井市風景優美，是一座受歡迎的城堡小鎮，擁有 Ichijodani Asakura Clan Ruins 等歷史遺產，自然風光十足。距離福井市不遠，有許多旅遊點，如“永平寺”，由國際權威旅遊指南分類為二星級，木造建築有八百年的歷史，屬禪門曹洞宗，參天群松環繞，令人心情平靜，一滌塵囂。福井市擁有豐富的自然風光，美食。福井市自豪地保留著歷史遺跡，並製作了歷史人物。福井的傳統在其悠久的歷史中得到了發展，至今仍然存在。

亦參訪福井縣恐龍博物館，因為該縣發現了許多恐龍化石，縣立恐龍博物館位於勝山市，是世界三大恐龍博物館之一，是一個非常獨特的地方，連 JR 福井車站都以恐龍為主題設計打造，可以說是福井縣的代表，每年有超過 90 萬遊客來訪。同時該線也擁有精美的傳統工藝和工匠的優秀技術，Echizen Yaki 是一種流行的陶器，以其簡約和樸實的色調而聞名，Echizen Washi 在日本的所有紙張中都很少見。迷人的噴漆黑色或朱紅色塗層，鑲嵌金色，越前漆體現了文化和精緻。還品嘗了福井種植的蕎麥麵，用石磨麵粉製作的手工蕎麥麵具有濃郁的味道，煮沸的熱蕎麥麵被冷水冷卻，並與高湯和日本蘿蔔一起食用，這種獨特的飲食方式被廣泛稱為福井的典型飲食文化。當然，福井市擁有美味的水和米飯，擁有超過 10 種不同的清酒，每種清酒都有自己的特色，有不同的口味和香氣。

心得及建議

本次參加之國際研討會為第 32 屆太空科技與科學國際研討會(32nd International Symposium on Space Technology and Science)，超過 1,000 名參與會議的論文發表者及聽講者(包含學者教授、研究生、產業界研究人員）遍及世界各國，ISTS 研討會探討領域甚廣，是一個關於太空技術和科學的國際研討會，涵蓋了與空間有關的幾乎所有學科，舉凡太空領域的航空器、火箭和衛星等等均涵蓋在內，飛行器在高重力和高速度下會產生極高強度和高頻率的暫態機械行為，容易造成內、外部原件材料結構損壞，故複合材料受衝擊時分析在太空領域的設計是重要的研究議題。本次以「理論分析模型預測功能梯度陶瓷複合材料受衝擊時行為」為題於此次研討會發表研究成果，藉由這次會議提供不同區域學者及業界代表面對面的交流機會，將新的研究方法與應用經驗相互觀摩學習，可進一步建立業務或研究關係，及尋找未來合作的夥伴。會議的目的期望能對相關領域的最新科學知識交流有所貢獻。參加此次研討會屬難得的機會，除可藉由參與國際研討會吸取新知外，並可促發對材料衝擊分析未來應用的新想法，以精進研究能力。

另除相關研究領域外，本次會議投稿篇數為 1,000 餘篇，學術討論範圍計有：化學推進和吸氣式發動機、材料與結構、航天動力學，導航制導與控制、流體動力學和氣動熱力學、小衛星、航天運輸、微重力科學與技術、熱控、衛星通信廣播和導航、科學和技術促進人類與機器人太空探索、探空火箭、地球觀測、太空生命科學、航天動力系統、太空環境和碎片、系統工程和信息技術、航天教育和推廣為全民利益、太空法律，政策和國際合作、安全與任務等 20 幾項主軸，極為豐富。

航太科技可說是科技發展的領頭羊，從事尖端的研究，不能僅以市場需求考量。政府以前瞻的規劃，整合優秀的人才，給予足夠的支持，或可讓我國在此領域和世界接軌，並延伸至國內的相關產業及研究上，藉以提高我國之競爭力。

以觀摩學習的態度參加此次國際研討會，深深感覺教學與研究所擔負的責任；看到國際間各學者最近研究成果，對材料材質改善、量測技術、性能提升，設計創意等都不遺餘力，個人認為應多鼓勵我國相關學者與研究人員參加類似之國際交流會議，讓從事科技研究人員拓展視野、得到更多的啟發，期能立足於競爭的世界舞台。同時，深感英文能力表達之重要性，此後亦當持續鼓勵研究生參加國際研討會，以培養其表達與溝通的能力。

附件一：獲邀發表論文簡報

32nd ISTS

Impact Behavior of a Functionally Graded Ceramic Composite Based on Derived Theoretical Analysis Model

Presenter：Yu-Liang Chen
Professor
National Defense University, Taiwan

Outline

1. Introduction
2. Theoretical analysis model
3. Model verification
4. Experimental plan
5. Results and discussion

1. Introduction(1/7)

- In 1987, the concept of gradient materials proposed, and officially named Functionally Graded Material (FGM).
- FGM was a new type of material in which the constituent elements of the material are continuously changed from one side in the thickness direction, and the properties and functions of the material are also changed in a gradient.

1. Introduction(2/7)

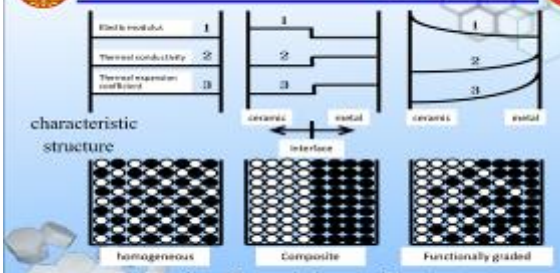

Functionally graded material structure and characteristic

1. Introduction(3/7)

- In nature, many animals and plants have evolved over a long period of time in order to adapt to environmental survival, and gradually formed various functional gradient materials, such as animal: shells and bones, plant: bamboos and trees.

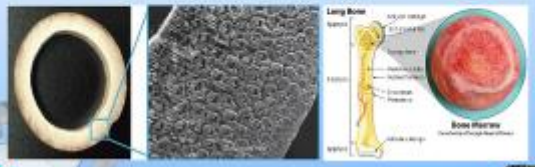

1. Introduction(4/7)

- Many studies in the field of impact resistance have shown that metal backplane can delay the formation of ceramic cones and slow down the crack growth of ceramics. Therefore, it has been studied by scholars that gradient ceramics can increase the toughness of ceramics and enhance the elastic properties of metal backplane.

1. Introduction(5/7)

- The ultimate goal of this study is to establish a high-speed impact functional gradient ceramic/metal theoretical model. Combining the impact and failure modes of the two distinct performance materials, the residual velocity of the warhead can be predicted.

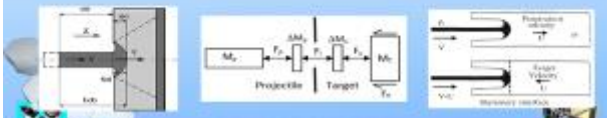

2. Theoretical analysis model

Tate equation (modified Bernoulli equation)

$$Y_p + \frac{1}{2}\rho_p (V-U)^2 = R_t + \frac{1}{2}\rho_t U^2 \qquad (1)$$

ρ_p, ρ_t : density of bullet & target

Y_p, R_t : dynamic yield strength of bullet & target

V : bottom velocity of the bullet

U : the velocity at which the bullet penetrates

Bullet model

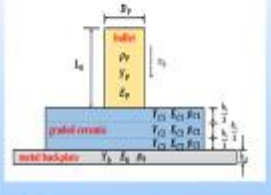

The bullet model: Assume that the projectile is a cylindrical flat-nose bullet

L_0: initial length

D_p: diameter

ρ_p: density

V_0: impact velocity

Y_p: dynamic yield strength

E_p: elastic modulus.

During the impact process, the deformation of the bullet is disregarded, and only the erosion of the mass (length) is considered.

Ceramic model

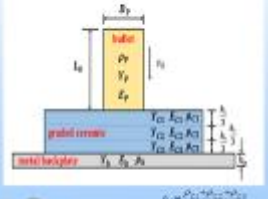

The ceramic model: Ceramic materials are brittle. Assume that the thickness of each layer of the graded ceramic is $\frac{h_c}{3}$, and the total thickness is h_c. The densities of the layers are ρ_{C1}、ρ_{C2}、ρ_{C3}, respectively, and the average density ρ_C. The elastic modulus values of the layers are E_{C1}, E_{C2}、E_{C3}, respectively, and the equivalent elastic modulus is E_C Their Poisson's ratios are v_{C1}、v_{C2}、v_{C3}, respectively. Their dynamic compressive strengths are Y_{C1}、Y_{C2}、Y_{C3}, respectively, and their average dynamic compressive strength is Y_C

Metal backplate model

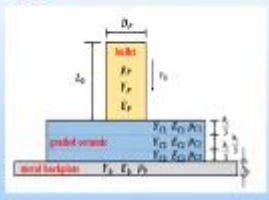

The metal backplate model: the backplate is made of elastic materials with a thickness of h_b, a density of ρ_b, an elastic modulus of E_b, and a yield strength of Y_b.

Bullet (1/4)

- To simplify the model, flat-nose AP slugs were adopted in theoretical analysis, and they were further divided into two types.

Bullet (2/4)

t_{conoid} : conoid formation time

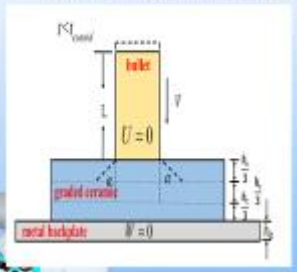

$$\begin{cases} \frac{dL}{dt} = -(V-U) = -V \\ U = 0 \\ t < t_{conoid} \end{cases} \quad (2)$$

$$\begin{cases} P = Y_p + \frac{1}{2}\rho_p (V-U)^2 = Y_p + \frac{1}{2}\rho_p V^2 \\ U = 0 \\ t < t_{conoid} \end{cases} \quad (3)$$

$$\frac{dV}{dt} = \frac{Y_p + \frac{1}{2}\rho_p V^2}{-\rho_p L} \quad (4)$$

Bullet (3/4)

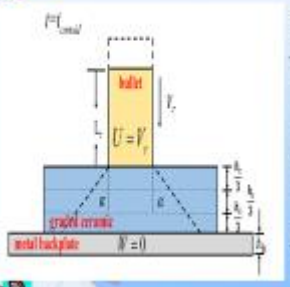

$$\begin{cases} \frac{dL}{dt} = -(V-U) = 0 \\ U = V = V_c \\ t = t_{conoid} \end{cases} \quad (5)$$

$$\begin{cases} P = Y_C + \frac{1}{2}\rho_C V^2 \\ V = U \end{cases} \quad (6)$$

$$\frac{dV}{dt} = \frac{Y_C + \frac{1}{2}\rho_C V^2}{-\rho_p L_p} \quad (7)$$

Bullet (4/4)

- Den Reijer analyzed ceramic conoids. He assumed that the compressive stress wave penetrated the entire ceramic structure from the point of impact, engendering cracks in the ceramic layers. When the cracks expand to the entire ceramic structure, a ceramic conoid forms. The time at which a ceramic conoid forms is :

$$t_{conoid} = \frac{h_C}{u_{long}} + \frac{h_C}{v_{crack}} = \frac{6h_C}{u_{long}} \quad (8)$$

$$t_{conoid} = t_{c1} + t_{c2} + t_{c3} = \frac{2h_C}{u_1} + \frac{2h_C}{u_2} + \frac{2h_C}{u_3} \quad (9)$$

Ceramic conoid (1/3)

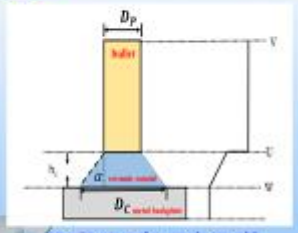

$$D_C = D_P + 2h_C \tan\alpha \quad (10)$$

$$\frac{dh_C}{dt} = -(U-W) \quad (11)$$

$$\frac{dD_C}{dt} = -2\tan\alpha (U-W) \quad (12)$$

Momentum of ceramic conoid

$$P_C = \frac{1}{48}\pi\rho_C h_C [U(3D_P^2 + D_C^2 + 2D_P D_C) + W(D_C^2 + 3D_C^2 + 2D_P D_C)] \quad (13)$$

Ceramic conoid (2/3)

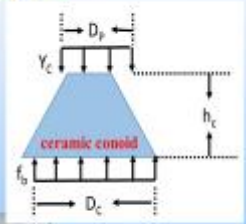

$$\frac{dP_C}{dt} = \pi(\frac{D_P}{2})^2 Y_C - \pi(\frac{D_C}{2})^2 f_b \quad (14)$$

$$\frac{\partial P_C}{\partial h_C}\frac{dh_C}{dt} + \frac{\partial P_C}{\partial D_C}\frac{dD_C}{dt} + \frac{\partial P_C}{\partial U}\frac{dU}{dt} + \frac{\partial P_C}{\partial W}\frac{dW}{dt} = \frac{1}{4}\pi(D_P^2 Y_C - D_C^2 f_b) \quad (15)$$

Ceramic conoid (3/3)

- According to the experiments of Den Reijer, α is generally between 60° and 65°. This study assumed α = 63.44°; therefore, tan α = 2.
- According to the change of the strength of the broken ceramic cone by Wilkin, the strength Y_C of the broken ceramic cone is related to the upper and lower moving velocities U and W of the ceramic cone.

$$Y_C = Y_{C0}(\frac{U-W}{U_0})^2 \quad (16)$$

Metal backplate (1/7)

- After the first stage, the ceramic conoid is separated from the ceramic plate along crack lines. The eroded bullet and the ceramic conoid move together on the metal backplate, causing tensile and bending deformation.

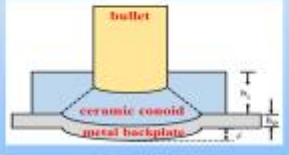

δ : Displacement of the center of the metal backing plate

Metal backplate (2/7)

- According to the theory proposed by Woodward et al., the plastic deformation energy required for the backplate tensile and bending deformation presented here as

$$E_j = \pi h_b \delta Y_b (\frac{2}{3}h_b + \frac{1}{2}\delta) \quad (17)$$

- During the process of deformation, the pressure of the metal backplate receives from the ceramic conoid is f_b, and the work it produces is

$$T = \pi(\frac{D_C}{2})^2 f_b \delta \quad (18)$$

Metal backplate (3/7)

- The kinetic energy in the central area of the metal backplate is:

$$E_K = \frac{1}{2}[\pi(\frac{D_b}{2})^2 h_b \rho_b]W^2 \qquad \frac{d\delta}{dt} = W \qquad (19)$$

- According to the conservation of energy, the power of the ceramic conoid to the metal backplane is equal to the rate of change of kinetic energy in the central region of the metal backplate plus the rate of change of plastic energy.

$$\frac{dT}{dt} = \frac{dE_J}{dt} + \frac{dE_K}{dt} \qquad (20)$$

Metal backplate (4/7)

- Simplifying, we obtain

$$\frac{dW}{dt} = \frac{D_p^2 Y_c - (\frac{4}{\pi}\frac{dP_c}{dt}) - 4h_b Y_b(\frac{2}{3}h_b + \delta)}{D_b^2 h_b \rho_b} \qquad (21)$$

- According to results from Zaera, when the penetration velocity U is close to the velocity of the metal W, the target plate failed, even it is not perforated. Therefore, the failure criterion is $U = W$. In this plug-type penetration mode, the plug and the bullet move forward at the same velocity. This design is suitable for low impact velocity, and in this study, this model was utilized for thick metal backplates.

Metal backplate (5/7)

- The second type is the petal type. If the impact velocity is much faster than the ballistic limit velocity, the bullet will completely penetrate the ceramic structure and will contact the metal backplate without causing substantial bending to the backplate.

Metal backplate (6/7)

- Therefore, Eq. (18) was revised to show the work of the bullet on the metal backplate as:

$$T = \pi(\frac{D_p}{2})^2 Y_b \delta \qquad (22)$$

- The kinetic energy in the central area of the metal backplate were adjusted as:

$$E_K = \frac{1}{2} M_b W^2 \qquad (23)$$

Metal backplate (7/7)

- According to the conservation of energy, the power of the bullet to the metal backplane is equal to the rate of change of kinetic energy in the central region of the metal backplate plus the rate of change in plastic work.

$$\frac{dW}{dt} = \frac{Y_b D_p^2 - 4h_b Y_b(\frac{2}{3}h_b + \delta)}{\rho_b[D_b^2 h_b - D_p^2(h_b - h_{bf})]} \qquad (24)$$

- when the thickness of the center of the metal plate is reduced to 0, the target plate fails, or $h_{bf} = 0$
- The petal-type penetration mode was employed for thin metal backplates in this study.

3. Model verification (1/4)

- From the theoretical analysis model established above, the differential equations are finally summarized. In this study, the differential equations are used to substitute the material parameters of the functionally graded ceramics and solved by the Matlab solver ode45.
- In order to compare the theoretical analysis results with those of other researches, this study firstly substitutes the gradient ceramic part of the theoretical model with the non-gradient ceramic material parameters to obtain the special solution and compared with the theoretical model of Dr. Zhang Xiao-qing's thesis and the experimental results of Den Reijer. The thesis analyzes the deformation of the projectile while considering the deformation of the target. This study considers the erosion and wear of the projectile without considering the deformation of the projectile.

3. Model verification (2/4)

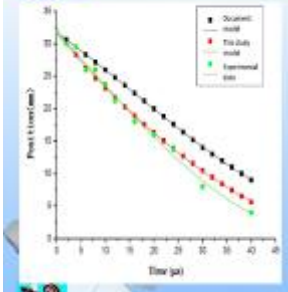

From the coordinate change diagram at bottom of the projectile, it can be seen that the theoretical analysis model established in this study is more accurately reflects the impact process of the bullet impacting the ceramic/metal composite target.

3. Model verification (3/4)

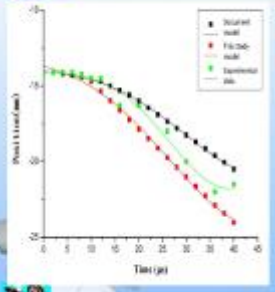

From the coordinate change diagram at the center position of the metal back plate, the experimental data is between the literature model and the research model. The experimental data is close to the research model at 36 μs, and rebounds at 40 μs.

3. Model verification (4/4)

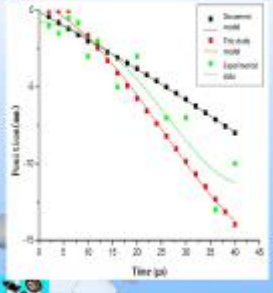

From the coordinate change diagram at the contact surface of the projectile, the experimental data is between the literature model and the research model. The experimental data is close to the research model at 36 μs, and rebounds at 40 μs.

4. Experimental plan(1/4)

- A key point in selecting FGMs for armor is that the coefficients of thermal expansion are similar. Therefore, the ceramics used in this study were composed of high-purity Al_2O_3 and ZrO_2 to avoid stress concentration and delamination.
- The FGM plates in this study were divided into three layers in the direction of thickness. The material proportion in the first layer composed Al_2O_3 (100%), Al_2O_3 (90%) and ZrO_2 (10%) in the second layer, and Al_2O_3 (80%) and ZrO_2 (20%) in the third layer.

4. Experimental plan(2/4)

- Backplates made of 6061-T6 Al aluminum alloy were adopted. In theoretical model calculations, only the thickness of the aluminum alloy backplate varied. When the thickness between 1 mm to 3 mm, the failure mode of the aluminum backplate was more similar to petal-type and could be described using Eq.(24). However, when the thickness of the backplate was 4 mm or more, then Eq.(21) were adequate because the failure would be a plug-type.

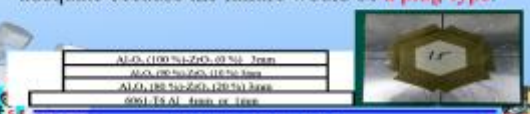

4. Experimental plan(3/4)

Ballistic test equipments

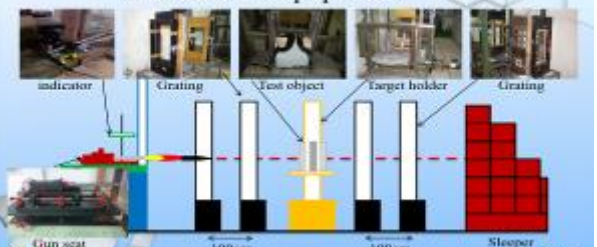

4. Experimental plan(4/4)

- The ballistic test was executed by using 0.30" armor-piercing (AP) bullet.
- By measuring the average initial velocity, the average residual velocity, and the residual mass of the bullet to verify the derived theoretical model.

5. Results and discussion

(1)Experimental results

(2)Theoretical analysis results

(3)Comparisons of the results from analysis model and experiments

A.Comparisons of the residual velocity

B.Comparisons of the residual mass

C.Comparisons of the ceramic conoid angle

D.Comparisons of the plug and petal types on the metal backplate

(1) Experimental results

- Specimens were divided into four types, three tests were conducted on each type of specimen. The table summarizes the experimental results.

No.	Target plate	Average initial velocity (m/s)	Average residual velocity (m/s)	Initial mass of the bullet (g)	Initial steel mass in the bullet(g)	Residual steel mass in the bullet(g)	Residual copper mass in the bullet(g)
1	10%-333 FGM/ 4 mm Al backplate	844.0	301.7	10.58	5.187	3.38	2.289
2	10%-333 FGM/ 1 mm Al backplate	850.7	489.9	10.58	5.187	3.78	4.466
3	5%-333 FGM/ 4 mm Al backplate	847.7	297.9	10.58	5.187	3.55	2.553
4	5%-333 FGM/ 1 mm Al backplate	842.8	473.7	10.58	5.187	3.79	2.793

10%-333 FGM/1 mm Al backplate

10%-333 FGM/4 mm Al backplate

(2)Theoretical analysis results(1/2)

- The material parameters used in this theoretical model were adopted from Huang's dissertation.
- Using the Matlab ode45 solver, the differential equations in the theoretical model are solved simultaneously. The rate of change of velocity and projectile length were obtained.

(2)Theoretical analysis results(2/2)

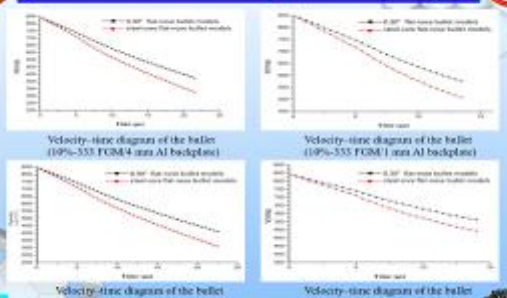

Velocity–time diagram of the bullet (10%-333 FGM/4 mm Al backplate)

Velocity–time diagram of the bullet (10%-333 FGM/1 mm Al backplate)

Velocity–time diagram of the bullet (5%-333 FGM/4 mm Al backplate)

Velocity–time diagram of the bullet (5%-333 FGM/4 mm Al backplate)

A. Comparisons of the residual velocity(1/2)

- The comparisons of residual velocities obtained from four types of target plate ballistic test results and from the theoretical model are shown in table .

More reasonable

No.	Target plate	Ballistic experiment		Theoretical model				
		Average initial velocity (m/s)	Average residual velocity(m/s)	Initial velocity (m/s)	Residual velocity of the 0.30" flat-nose AP bullet(m/s)	Error (%)	Residual velocity of the steel core flat-nose AP bullet(m/s)	Error (%)
1	10%-333 FGM/ 4 mm Al backplate	844	301.7	844	425	28.93%	325	7.34%
2	10%-333 FGM/ 1 mm Al backplate	850.7	489.9	850.7	578	14.99%	508	3.58%
3	5%-333 FGM/ 4 mm Al backplate	847.7	297.9	847.7	412	27.69%	311	4.21%
4	5%-333 FGM/ 1 mm Al backplate	842.8	473.7	842.8	562	15.73%	494	4.10%

A. Comparisons of the residual velocity(2/2)

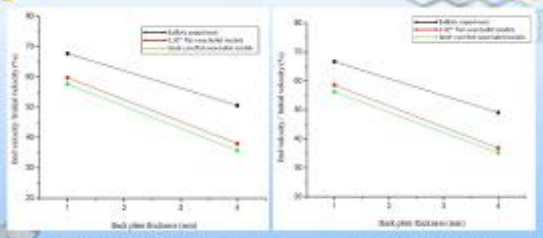

Velocity ratio-thickness diagram (10%-333 FGM/4 mm Al backplate)

Velocity ratio-thickness diagram (5%-333 FGM/4 mm Al backplate)

C.C.I.T. N.D.U. R.O.C.

B. Comparisons of the residual mass

- According to the aforementioned results, the theoretical steel core flat-nose AP model was selected. According to the theoretical model, the shortened length of the bullet was converted to the residual mass of the bullet, and that was compared with the ballistic test results shown in table.

No.	Target plate	Initial bullet mass (steel) (g)	Residual bullet mass (steel) (g)	Theoretical residual bullet mass (g)	residual bullet
1	10%-333 FGM/ 4 mm Al backplate	5.187	3.38	4.25	
2	10%-333 FGM/ 1 mm Al backplate	5.187	3.78	4.29	
3	5%-333 FGM/ 4 mm Al backplate	5.187	3.55	4.29	
4	5%-333 FGM/ 1 mm Al backplate	5.187	3.78	4.33	

C.C.I.T. N.D.U. R.O.C.

C. Comparisons of the ceramic conoid angle(1/2)

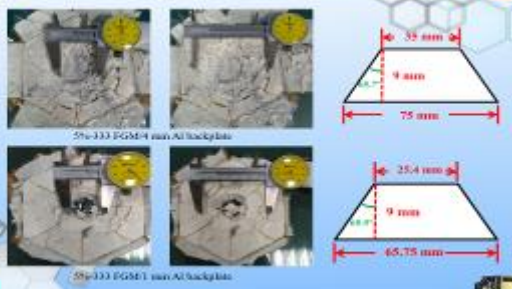

C.C.I.T. N.D.U. R.O.C.

C. Comparisons of the ceramic conid angle(2/2)

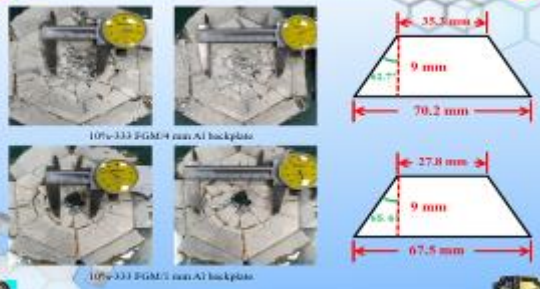

C.C.I.T. N.D.U. R.O.C.

D. Comparisons of the plug and petal types on the metal backplate (1/3)

- Theoretically, two failure types can be observed on the metal backplate, the plug type and the petal type. The comparison results revealed that when the aluminum alloy backplate was 4 mm in thickness, its mass was reduced by 2 g after the shooting, indicating that the stretching, bending, deformation, and extrusion caused mass loss.
- However, when the backplate was 1 mm thick, no mass loss after the shooting. Therefore, it is reasonable for this study to separate the aluminum alloy backplates into two categories in the theoretical analysis.

C.C.I.T. N.D.U. R.O.C.

D. Comparisons of the plug and petal types on the metal backplate (2/3)

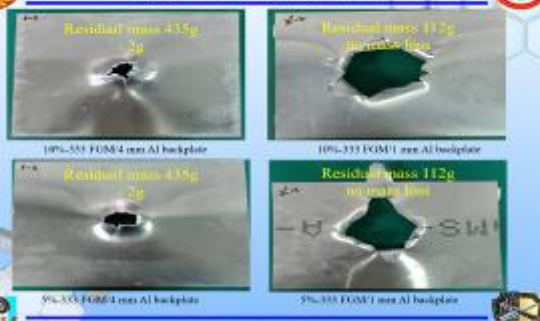

C.C.I.T. N.D.U. R.O.C.

D. Comparisons of the plug and petal types on the metal backplate (3/3)

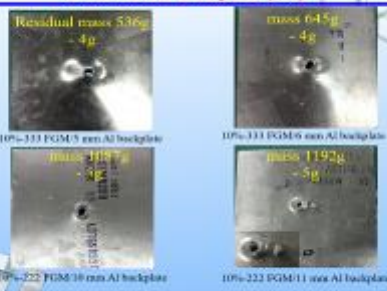

C.C.I.T. N.D.U. R.O.C.

S.B.L

Thanks for your attention

C.C.I.T. N.D.U. R.O.C.

附件二：參與交流研討之相關照片

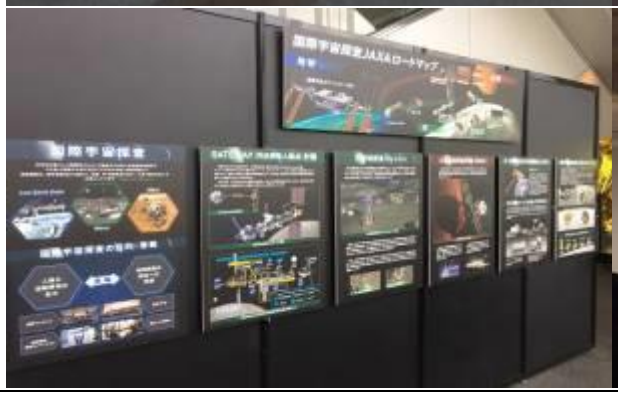


Room 601A